ACS APPLIED MATERIALS & INTERFACES

Research Article

Cite This: ACS Appl. Mater. Interfaces 2019, 11, 25547−25555

www.acsami.org

# Phonon−Grain-Boundary-Interaction-Mediated Thermal Transport in Two-Dimensional Polycrystalline $MoS_2$

Changpeng Lin,[†] Xiaobin Chen,*[,‡,§] and Xiaolong Zou*[,†]

[†]Shenzhen Geim Graphene Center (SGC), Tsinghua-Berkeley Shenzhen Institute (TBSI), Tsinghua University, Shenzhen 518055, People's Republic of China

[‡]School of Science and State Key Laboratory on Tunable Laser Technology and Ministry of Industry and Information Technology Key Lab of Micro-Nano Optoelectronic Information System, Harbin Institute of Technology, Shenzhen 518055, People's Republic of China

[§]Collaborative Innovation Center of Extreme Optics, Shanxi University, Taiyuan 030006, People's Republic of China

Supporting Information

**ABSTRACT:** Although dislocations and grain boundaries (GBs) are ubiquitous in large-scale $MoS_2$ samples, their interaction with phonons, which plays an important role in determining the lattice thermal conductivity of polycrystalline $MoS_2$, remains elusive. Here, we perform a systematic study of the heat transport in two-dimensional polycrystalline $MoS_2$ by both molecular dynamics simulation and atomic Green's function method. Our results indicate that the thermal boundary conductance of GBs of $MoS_2$ is in the range from $6.4 \times 10^8$ to $35.3 \times 10^8$ W m$^{-2}$ K$^{-1}$, which is closely correlated with the overlap between the vibrational density of states of GBs and those of the pristine lattice, as well as the GB energy. It is found that the GBs strongly scatter the phonons with frequency larger than 2 THz, accompanied by a pronounced phonon localization effect and significantly reduced phonon group velocities. Furthermore, by comparing the results from realistic polycrystalline $MoS_2$ to those from different theoretical models, we observe that the Casimir model is broken down and detailed phonon dynamics at a specific GB should be taken into account to accurately describe the phonon transport in polycrystalline materials. Our findings will provide useful guidelines for designing efficient thermoelectric and thermal management materials based on phonon−GB interaction.

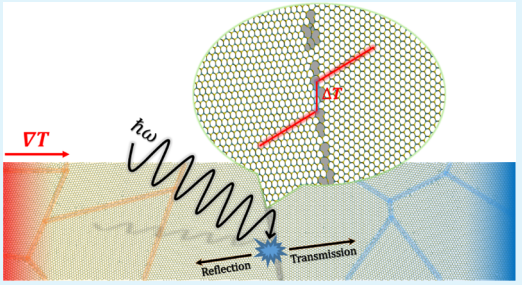


**KEYWORDS:** *phonon−grain boundary interaction, thermal boundary conductance, grain boundary, thermal conductivity, molecular dynamics, atomic Green's function*

## INTRODUCTION

As high Joule heating would lead to the premature failure of electronic devices, thermal transport is one of the crucial factors that influences their overall performance and stability. Particularly, lattice imperfections (e.g., impurities, vacancies, grain boundaries (GBs), dislocations, and interfaces) have significant impacts on the thermal performance of the materials.[1,2] Generally, nanoboundaries and interfaces would strongly filter low-frequency phonons, and point defects tend to scatter high-frequency phonons, while dislocations are shown to effectively impede the transport of mid-frequency phonons.[3−5] Both theoretical[6−15] and experimental investigations[16−24] have been widely performed to gain deep insights into the phonon-scattering mechanisms caused by structural defects. Although the effect of dislocations and grain boundaries (GBs) on heat conduction is a classical problem first discussed by Klemens[25] in 1955, the mechanisms of phonon−dislocation interaction have not been fully understood owing to the complex dislocation vibrations and the long-range elastic strain field.[26−30] Interestingly, extremely low thermal conductivities below the amorphous limit have been experimentally observed lately in polycrystalline materials.[31−33] Using classical molecular dynamics (MD) simulation, Zhou et al.[34] have studied the underlying mechanisms leading to the ultralow thermal conductivity of polycrystalline silicon nanowires. It is shown that the dominating heat carriers, diffusons, have very limited contributions to thermal transport. Meanwhile, the propagons, which can still carry the heat in amorphous states, are suppressed in polycrystalline structures due to the interferring phonon scattering and the strong localization of the vibrational modes in the middle- and high-frequency regions.[34] For the epitaxial nanocrystalline silicon with ultrasmall grain sizes (3−5 nm), Oyake et al.[33] also revealed the ultimate confinement of phonon propagation, which resulted in the ultralow thermal conductivity well below that of the amorphous state.

As a potential alternative to conventional three-dimensional materials for nanodevices, two-dimensional (2D) transition-

Received: April 9, 2019
Accepted: June 25, 2019
Published: June 25, 2019






DOI: 10.1021/acsami.9b06196
ACS Appl. Mater. Interfaces 2019, 11, 25547−25555

metal dichalcogenides (TMDs) have received a lot of research interest, among which thermal transport is a particularly important one. On the one hand, nanodevices built on these layered materials introduce a lot of interfaces. On the other hand, 2D TMDs prepared by the chemical vapor deposition (CVD) are usually polycrystalline, a natural outcome of nucleation, growth, and coalescence of grains.[35] As a consequence, the thermal transport behaviors of such samples could be strongly affected by phonon−GB scattering, leading to poor performance of nanodevices.

Two-dimensional TMDs such as $MoS_2$ have intricate dislocations and GBs due to the polarity of their constituent elements and the flexible Mo−S bonding coordination. Diverse structures of topological dislocations and GBs in TMDs were first predicted by Zou et al.[36,37] and subsequently validated in experimental observations.[38−40] Although the mechanical,[41−43] electronic,[36,37] and magnetic properties[44] of dislocations and GBs in $MoS_2$ have been systematically studied via theoretical simulations, the thermal transport through these topological dislocations and GBs is less investigated. Very recently, Sledzinska et al.[45,46] measured the thermal transport properties of polycrystalline $MoS_2$ thin films and recorded an extremely low thermal conductivity (~0.27 W $m^{-1}$ $K^{-1}$ at room temperature), which was nearly several hundred times lower than that of the pristine one.[47−49] With the aid of finite-element simulation, they attributed this unique phenomenon to the very low thermal conductance of GBs with different orientations. This explanation lacked the spectral information of phonon−GB interaction, especially the contributing phonon modes in the thermal transport through GBs. In addition, Mortazavi et al.[50] applied classical MD simulations to study the thermal boundary (Kapitza) conductance (TBC) of 5|7, 6|8, 4|6, and some high-angle GBs in 2D $MoS_2$ based on the ReaxFF force field.[51] In the same work, the finite-element modeling was also carried out to explore the thermal conductivity of polycrystalline $MoS_2$ as a function of grain size. Nevertheless, the understanding of thermal transport in polycrystalline $MoS_2$ still lacks the realistic model of polycrystalline structures and thus gives rise to a big discrepancy with experimental results. Directly studying the effective thermal conductivity of polycrystalline $MoS_2$ by MD simulation is still difficult because of the complex GB structures in $MoS_2$.[36−40] Importantly, the microscopic mechanisms of phonon−GB interaction that lead to extremely low thermal conductivity of polycrystalline $MoS_2$ is yet unknown, especially how phonons interact with different GBs on a mode-by-mode basis.

In this work, we perform systematic investigations on the phonon−GB interaction and thermal transport in polycrystalline $MoS_2$ by combining nonequilibrium molecular dynamics (NEMD) simulation and atomic (nonequilibrium) Green's function method. The calculated TBC of 12 types of GBs, either observed in experiments or predicted to be stable from first-principles calculations, shows a strong dependence on the overlap of vibrational density of states (VDOS) between GB and pristine lattice as well as on the GB energy. Detailed analysis on phonon transmission function indicates that GBs can significantly scatter the phonons with frequency larger than 2 THz, accompanied by a pronounced phonon localization effect and significantly reduced phonon group velocities. Furthermore, the well-known Casimir model[52,53] breaks down in the description of phonon−GB scattering, and the thermal conductivity of realistic polycrystalline $MoS_2$ constructed from Voronoi algorithm[54] is well below that predicted from phonon Boltzmann transport equation (BTE) with the Casimir boundary scattering included. We show that the mode-by-mode phonon transmissivity at GBs is crucial for accurately representing the phonon−GB-interaction-mediated thermal transport in polycrystalline materials. The atomic-scale simulations presented here will be helpful for understanding and accurately predicting the thermal transport properties of polycrystalline materials, as well as opening up new avenues for the rational defect engineering for advanced device applications and efficient thermal management.

## METHODOLOGY

According to experimental observations[38,40,55,56] and first-principles simulations,[36,37] diverse topological dislocations and GBs have been revealed in 2D TMDs. Here, 12 types of GBs (see the Supporting Information Section I) of $MoS_2$ are chosen to investigate the TBC and phonon−GB scattering, as they have been reported in experiments or found to be stable theoretically. While S5|7, Mo5|7, S4|6, and Mo6|8 GBs are in the group with a small tilt angle of 22°, the remaining GBs belong to another group with a high tilt angle of 60°. With a time step of 1.0 fs, all MD simulations are performed in large-scale atomic/molecular massively parallel simulator package[57] by using the second-generation reactive empirical bond-order (REBO) potential[58,59] to describe the interatomic interactions. Periodic boundary condition is applied in $y$ direction, while nonperiodic free boundary conditions are used in $x$ and $z$ directions with heat flux flowing along the $x$ direction. With lattice constants obtained from energy minimization, the systems of interest were first relaxed at 300 K in the NVT ensemble for 1 ns and then in the NVE ensemble for an additional 1 ns to have a better energy conservation. The TBC and thermal conductivity are calculated by Fourier's law in the NEMD simulation, where the left and right leads (with the lead length of 1.5 nm in all cases) of the system are coupled to hot and cold Nosé−Hoover[60,61] thermostats at the temperature of $T + \Delta T/2$ and $T - \Delta T/2$, respectively. All of the simulations are carried out at $T$ = 300 K and $\Delta T$ is chosen to be 40−60 K. We compute the time-averaged TBC and thermal conductivity after 8 ns of the total running time 20 ns, which has been shown to be long enough to reach the steady state of heat conduction and thus give rise to converged results.

## RESULTS AND DISCUSSION

The thermal conductivity of pristine monolayer $MoS_2$ is estimated first to validate the applicability of REBO force field for studying the thermal transport properties. Based on the thickness of 6.15 Å[62] for monolayer $MoS_2$, the room-temperature thermal conductivity of pristine one is 93 ± 3 W $m^{-1}$ $K^{-1}$ from NEMD simulation and 86 W $m^{-1}$ $K^{-1}$ from phonon BTE with lifetimes extracted from spectral energy density (SED) analysis[63,64] (see the Supporting Information Section III for technical details). These results are in excellent agreement with first-principles calculation (91 W $m^{-1}$ $K^{-1}$)[65] and experimental measurement (84 ± 17 W $m^{-1}$ $K^{-1}$)[47] for monolayer single-crystal $MoS_2$. In addition, the calculated phonon dispersion of pristine $MoS_2$ based on the REBO potential (see Figure S3 in the Supporting Information Section II) also agrees well with the results from the first principles.[66] Hence, it can be expected that the REBO force field is applicable to the investigation of thermal transport in $MoS_2$


DOI: 10.1021/acsami.9b06196
ACS Appl. Mater. Interfaces 2019, 11, 25547−25555

and can be further applied to investigate the phonon−GB interaction in polycrystalline $MoS_2$.

Figure 1a shows the temperature profile of S5|7 GB in polycrystalline $MoS_2$ from NEMD simulation. A small

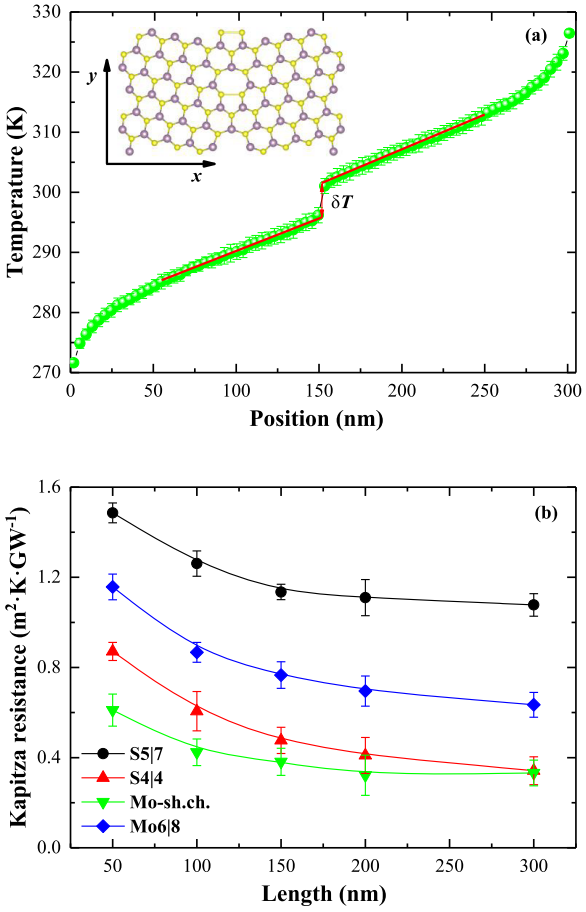


**Figure 1.** (a) Temperature profile of S5|7 GB in polycrystalline $MoS_2$ obtained from NEMD simulation. S5|7 GB is located in the middle of the sample with the typical temperature drop $\delta T$, and the red line represents the linear fitting. (b) The Kapitza resistance of S5|7, S4|4, Mo-sh.ch., and Mo6|8 GBs in polycrystalline $MoS_2$ as a function of sample length.

temperature drop $\delta T$ could be clearly noted at the middle of the sample (the position of S5|7 GB) and can be attributed to the phonon−GB scattering from both the elastic strain field around the GB[26,67,68] and the distinctly different GB vibrations[27] from the perfect counterpart. By fitting the linear regions of temperature profile separated by the middle GB as indicated by the red solid lines in Figure 1a, we can determine the temperature drop $\delta T$ to be roughly 5.71 K for a 300 nm × 10 nm sample containing a single S5|7 GB. The TBC $\sigma$ of S5|7 GB can be readily obtained via the Fourier's law, $\sigma = J/\delta T = 9.28 \times 10^8$ W m$^{-2}$ K$^{-1}$, where $J$ is the heat flux through the GB ($52.97 \times 10^8$ W m$^{-2}$ for this case). We have systematically tested the chosen simulation parameters in NEMD such as the temperature difference $\Delta T$, the number of used bins, and the width and the length of sample. These parameters have very limited influence on the calculated TBC except the sample length. To illustrate the effect of sample length on the TBC, the length-dependent Kapitza resistances (inverse of TBC) of the S5|7, S4|4, Mo-shifted chevron (Mo-sh.ch.), and Mo6|8 GBs are plotted in Figure 1b. The size effect arises when the intrinsic phonon mean free path in $MoS_2$ is remarkably longer than the simulated sample length.[69,70] The Kapitza resistances of all the four types of GBs at first decrease rapidly with the increasing sample length and become almost saturated at the sample length of 300 nm. For S4|4 and Mo-sh.ch. GBs, the temperature drop for the samples with length of 300 nm is very small, ∼2 K, which leads to a larger TBC fluctuation. Based on such a tiny temperature drop, it is suggested that S4|4 and Mo-sh.ch. GBs are nearly transparent to heat transport, exhibiting smallest thermal resistances. As the TBC of GBs almost converges with the sample length of 300 nm, our subsequent predictions of TBC for various GBs in polycrystalline $MoS_2$ are based on the sample size of 300 nm × 10 nm.

The TBCs of the selected 12 types of GBs in polycrystalline $MoS_2$ are summarized in Figure 2 as a function of VDOS

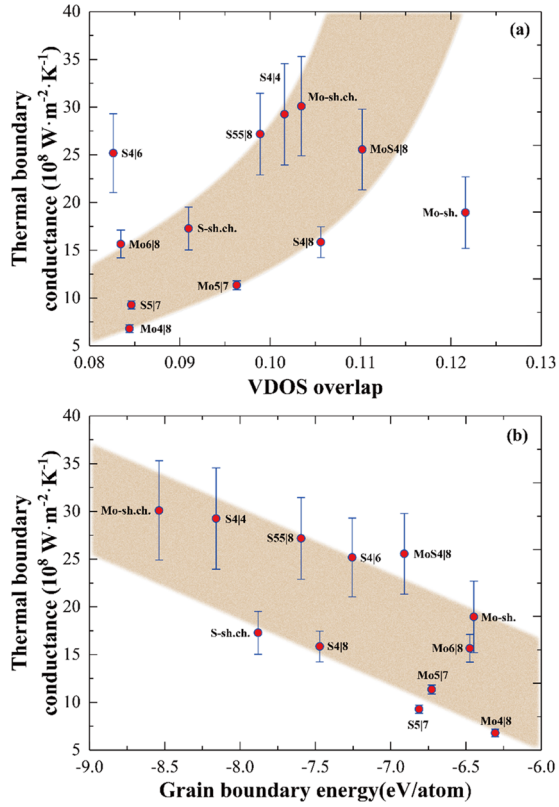


**Figure 2.** Thermal boundary conductance for 12 types of GBs in polycrystalline $MoS_2$ as a function of (a) VDOS overlap and (b) GB energy. The shadow area is used to guide the eyes.

overlap and GB energy. The VDOS overlap $S$ between the GB and grain vibrations is defined as[13,71]

$$S = \frac{\int_0^\infty D_G(\omega) D_B(\omega) d\omega}{\int_0^\infty D_G(\omega) d\omega \int_0^\infty D_B(\omega) d\omega} \quad (1)$$

where $D_G(\omega)$ and $D_B(\omega)$ are the VDOS of the grain and GB vibrations, respectively. VDOS is calculated by taking the Fourier transform of normalized velocity autocorrelation function $\langle \sum_i v_i(0) v_i(t) \rangle / \langle \sum_i v_i(0) v_i(0) \rangle$[72] of the specific atomic group either belonging to grain or GB. The $\langle \cdots \rangle$ denotes the time average and $v_i(t)$ is the velocity of atom $i$ at time $t$. As seen from Figure 2a, the TBC of different GBs reflects a positive correlation with VDOS overlap. The overlap of VDOS is believed to serve as a phonon bridge to build the heat-


DOI: 10.1021/acsami.9b06196
ACS Appl. Mater. Interfaces 2019, 11, 25547−25555

transfer channels through mismatched interfaces or materials,[13,71,73] benefitting the thermal transport through the GBs in polycrystalline materials as well. As for the GB energy, it also closely relates to thermal transport because it largely characterizes the change of bonding environment around a GB. The GBs in TMDs with different orientations could be either metal-rich or S-rich. In these cases, the GB energy depends on the free energy (i.e., chemical potential) of excess Mo or S atoms.[36,37] To determine the chemical−potential-dependent GB energy using MD simulations is very difficult. Thus, we compute the average GB energy by directly summing the contributions of kinetic and potential energies of the atoms explicitly showing the GB geometry. Our simple estimation of the GB energy shows that S4|4 and Mo-sh.ch. GBs are relatively more stable than others, which is in accordance with the conclusions from the first-principles calculations.[37] According to Figure 2b, the estimated TBC of diverse GBs also displays a clear tendency with the GB energy, increasing remarkably as the GB energy becomes lower. A lower GB energy implies a more stable GB, which further indicates a stronger chemical bonding at the GB and thus facilitates the heat transport. The obvious dependence of Kapitza resistance on various chemical bondings is consistent with previous results on different interfaces.[74,75] It is worth noting that the TBC of some GBs deviates from the predicted trend in regard to the VDOS overlap or GB energy because other factors such as the distribution of elastic strain field[13,26] could affect the thermal transport through GBs as well. Importantly, our predictions for the TBC of 12 types of GBs give a reasonable range for TBC of the diverse topological dislocations and GBs in polycrystalline $MoS_2$, from $6.4 \times 10^8$ W m$^{-2}$ K$^{-1}$ of Mo4|8 to $35.3 \times 10^8$ W m$^{-2}$ K$^{-1}$ of Mo-sh.ch. and S4|4. Although different interatomic potentials are adopted, these results have similar magnitudes as the results obtained by Mortazavi et al.,[50] who studied some of the GBs considered in this work. Compared with the TBC of 5|7 GB in graphene ($150-450 \times 10^8$ W m$^{-2}$ K$^{-1}$)[8] and h-BN ($100-120 \times 10^8$ W m$^{-2}$ K$^{-1}$),[76] the dislocations and GBs of $MoS_2$ exhibit surprisingly low TBC, which could be attributed to the intrinsic low thermal conductivity of pristine $MoS_2$.[47,65]

To understand the phonon−GB interaction in polycrystalline $MoS_2$ on a mode-by-mode basis, atomic Green's function method[77,78] (see the Supporting Information Section IV for detailed implementation of atomic Green's function) is employed to obtain the frequency-dependent phonon transmission function through GBs, as shown in Figure 3a,b for S4|4 and Mo4|8, respectively, which have the largest and smallest TBC, respectively. S4|4 GB strongly scatters the phonons with frequency between roughly 4 and 12 THz (the mid-frequency range), which is in line with the phenomenological model by Klemens.[25] The low-frequency phonons (<2−3 THz) have extremely long wavelength compared with the characteristic size of GB cores, and thus become "invisible" to the vibrations of GBs. This portion of long-wavelength modes in phonon dispersion travel ballistically through GBs without much scattering,[15] leading to high phonon transmissivity above 0.9. For Mo4|8 GB, phonons with frequency larger than 2 THz are more prominently scattered. Analogous results can be also found for other types of GBs in polycrystalline $MoS_2$, which are shown in the Supporting Information Section V. In addition, we show that acoustic phonons dominate the heat transport in pristine $MoS_2$ monolayer, contributing to 97% of the total thermal conductivity at room temperature, with 67%

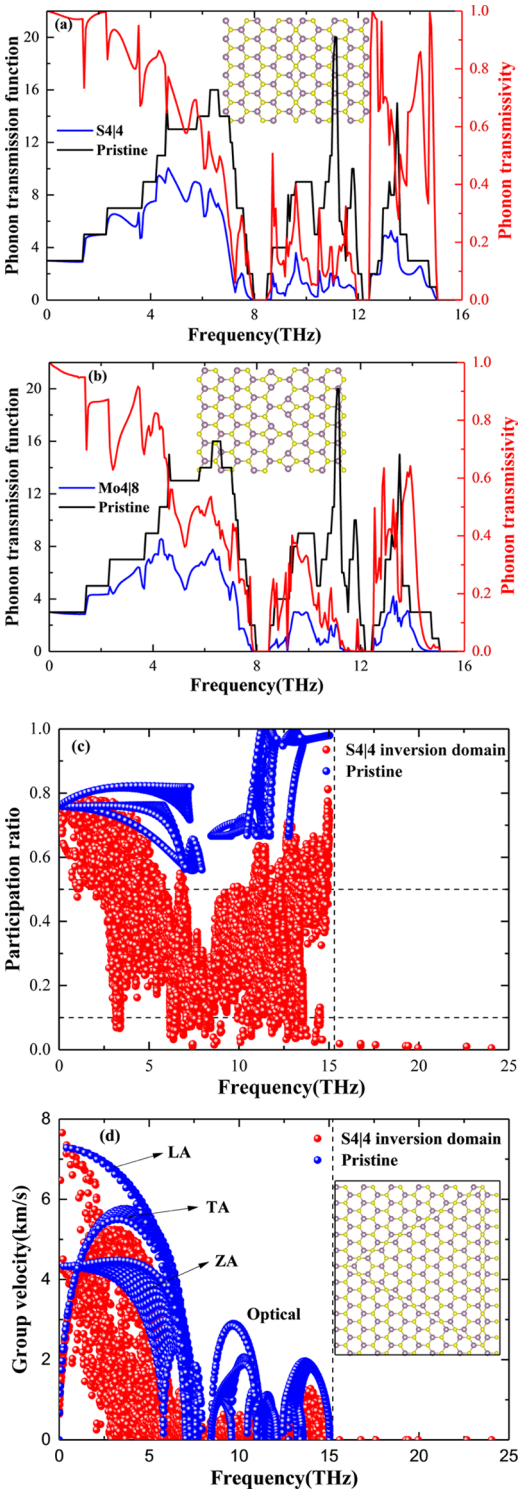


**Figure 3.** Frequency-dependent phonon transmission function/transmissivity of (a) S4|4 and (b) Mo4|8 GBs. The phonon transmission function of pristine $MoS_2$ is plotted for comparison. The red solid line is phonon transmissivity defined as the phonon transmission function of GB divided by the pristine one, belonging to the right vertical axis. (c) Participation ratio and (d) phonon group velocities of the S4|4 inversion domain and pristine $MoS_2$. The highest frequency of phonons in pristine $MoS_2$ is shown as vertical dash line and the 0.1 and 0.5 values of participation ratio are drawn as two horizontal dash lines. The different phonon branches, namely, longitudinal acoustic, transverse acoustic, flexural acoustic, and optical phonon are labeled for the pristine $MoS_2$ in (d).



DOI: 10.1021/acsami.9b06196
ACS Appl. Mater. Interfaces 2019, 11, 25547−25555

from the phonons with frequency larger than 2 THz (see phonon SED analysis in the Supporting Information Section III). Therefore, the thermal conductivity of polycrystalline $MoS_2$ is expected to be significantly reduced by phonon−GB scattering, as already reflected in the phonon transmissivity of S4|4 and Mo4|8 in Figure 3a,b. Further calculations on spectral contributions to TBC according the Landauer formula[79] (see atomic Green's function method in the Supporting Information Section IV) indicate that acoustic phonons between nearly 2 and 7 THz are responsible for the heat transport through the GBs in polycrystalline $MoS_2$ at room temperature.

To further understand the thermal transport in polycrystalline $MoS_2$, we construct the triangular inversion domain, which is composed of S4|4 GBs (see the insert of Figure 3d) and often reported in experiments.[55,56] The computed participation ratio $P_{\mathbf{q}\nu}$ and phonon group velocities $\boldsymbol{\upsilon}_{\mathbf{q}\nu} = \partial\omega_{\mathbf{q}\nu}/\partial\mathbf{q}$ along with those of the pristine one are shown in Figure 3c,d. The detailed expression of the participation ratio can be written as[34]

$$P_{\mathbf{q}\nu} = \frac{1}{N_s \sum_i \left(\sum_\alpha e^*_{i\alpha,\mathbf{q}\nu} e_{i\alpha,\mathbf{q}\nu}\right)^2} \tag{2}$$

where $N_s$ is the number of atoms in the unit cell, $e_{i\alpha,\mathbf{q}\nu}$ is the eigenvector along $\alpha$ direction ($\alpha = x, y, z$) of the $i$th atom in the unit cell associated with the vibrational mode at the wavevector $\mathbf{q}$ and band index $\nu$, and * denotes the complex conjugate operation. According to eq 2, it is straightforward that the participation ratio $P_{\mathbf{q}\nu}$ has the value between $1/N_s$ and 1, describing the percentage of atoms in a system participating in the given vibrational mode. In other words, $P_{\mathbf{q}\nu}$ becomes $O(1)$ when all of the atoms in the chosen unit cell participate in a vibrational mode and becomes $O(1/N_s)$ when only one atom contributes to a vibrational mode. As can be seen in Figure 3c, the vibrational modes in pristine $MoS_2$ are all extended modes in the whole frequency range with $P_{\mathbf{q}\nu}$ greater than 0.5, and it is reasonable to treat them as phonons or propagons in such a perfect lattice.[80,81] In contrast, most of vibrational modes in the S4|4 inversion domain changed into diffusons[80,81] with smaller $P_{\mathbf{q}\nu}$ well below 0.5, indicating a significant phonon localization effect induced by GB cores and strong phonon−GB scattering, as well as appreciable phonon interference from different GBs. Nevertheless, some phonon-like modes (propagons) could be still maintained in the low-frequency region (i.e., <2 THz) of the S4|4 inversion domain because these vibrational modes have very long wavelength and are less affected by GBs, thus contributing remarkably to thermal conductivity of polycrystalline $MoS_2$. Meanwhile, the strong phonon localization effect gives rise to the pronounced reduction in phonon group velocities of the S4|4 inversion domain, especially for acoustic phonons, which can be easily noticed in Figure 3d for phonon modes with frequency higher than 2 THz. This is also consistent with the results of phonon transmission analysis. Above the highest frequency of phonons in pristine $MoS_2$, there still exist some vibrational modes, which are nonpropagating with zero group velocities and completely localized (locons,[80,81] $P_{\mathbf{q}\nu} < 0.1$), arising from the vibrations of dislocations and GBs. In fact, the vibrational modes of dislocations and GBs can be found in the whole frequency range.[27] They may additionally scatter acoustic phonons, thus further hindering the heat conduction in polycrystalline $MoS_2$. Similar results are also found for other typical GBs, Supporting Information Section VI.

Now, we turn to study the scaling behavior of the thermal conductivity of polycrystalline $MoS_2$ as a function of grain size. The polycrystalline samples of $MoS_2$ are constructed by Voronoi algorithm[54] (see the Supporting Information Section VII for details). The thermal conductivities of polycrystalline $MoS_2$ from the Voronoi algorithm (denoted as realistic polycrystalline $MoS_2$) with grain sizes of 3, 6, and 12 nm are calculated from NEMD simulation and are shown in Figure 4.

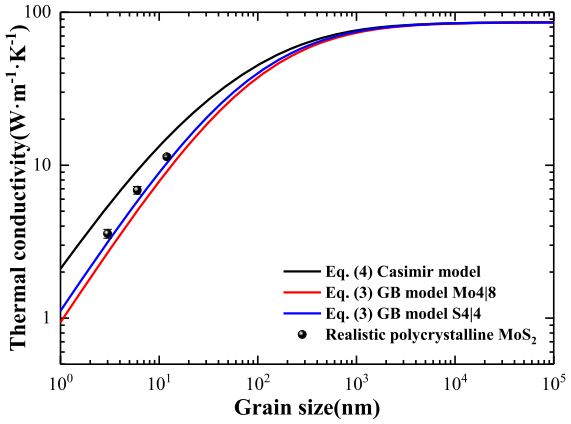


**Figure 4.** Thermal conductivity of polycrystalline $MoS_2$ as a function of grain size. The realistic polycrystalline $MoS_2$ (discrete black points) is constructed from Voronoi algorithm with the thermal conductivity determined from NEMD simulations. The solid lines are obtained from phonon BTE under single-mode relaxation time approximation by including the GB scattering described by the Casimir model or the GB model in the main text. "GB model Mo4|8/S4|4" indicates the phonon transmissivity through Mo4|8/S4|4 is used in the GB model to calculate the GB scattering rate.

For comparison, Figure 4 also presents the results predicted by phonon BTE via including the GB scattering, which is either described by the well-known Casimir model[52] or the recently developed analytical model[82,83] for GB scattering (denoted as the GB model). In the GB model, the GB scattering rate $\tau_{gb}^{-1}$ can be defined as

$$\tau_{gb}^{-1} = \left[\left(\frac{\frac{3}{4}\xi(\omega)}{1-\xi(\omega)}\right)^{-1} + \left(\frac{1+p(\omega)}{1-p(\omega)}\right)^{-1}\right] D_{avg}^{-1} v_{g,\alpha} \tag{3}$$

where $\xi(\omega)$ is the modal phonon transmissivity through GBs obtained from atomic Green's function (Figure 3a,b), $p(\omega)$ is the frequency-dependent specularity parameter measuring the proportion of specularly scattered phonons, $D_{avg}$ is the average grain size of polycrystalline sample, and $v_{g,\alpha}$ is the phonon group velocity along $\alpha$ direction ($\alpha = x, y, z$). By approximating the polycrystalline structure as a superlattice nanowire, eq 3 can be understood by incorporating the effects of GB scattering both perpendicular and parallel to the transport direction using the Matthiessen's rule. Furthermore, omitting the first phonon-transmission-dependent term at the right-hand side of eq 3, the phonon-boundary-scattering rate in the Casimir model can be easily derived as

$$\tau_C^{-1} = \frac{1-p(\omega)}{1+p(\omega)} D_{avg}^{-1} v_{g,\alpha} \tag{4}$$

This model assumes the characteristic grain size $D_{avg}$ as the effective mean free path of phonons limited by GB scattering,


DOI: 10.1021/acsami.9b06196
ACS Appl. Mater. Interfaces 2019, 11, 25547−25555

which is widely applied in phonon BTE calculations to include the size effect.[65,84,85] As the specularity parameter $p(\omega)$ depends on both the roughness of studied GB and phonon frequency, it is usually determined from the Ziman formula.[85] For simplicity, we choose it as zero for all phonon modes, representing fully diffusive scattering at GBs.[65,84] (The detailed description for the thermal conductivity of polycrystalline $MoS_2$ predicted from phonon BTE via including GB scattering can be found in the Supporting Information Section III). From Figure 4, it can be clearly seen that thermal conductivity of realistic polycrystalline $MoS_2$ is well below the Casimir limit, suggesting the Casimir model fails in describing the phonon−GB scattering in polycrystalline materials. This intriguing phenomenon can be understood from the fact that the Casimir model does not take into account any information of phonon transmission or reflection at GBs, an important phonon behavior strongly altered by different interfaces or GBs, and thus would be no longer valid in the case of polycrystalline materials. In contrast, the GB model that explicitly considers the frequency-dependent phonon transmissivity at a specific GB (S4|4 or Mo4|8 in Figure 4) gives a more reasonable approximation to the thermal conductivity of realistic polycrystalline $MoS_2$. Interestingly, the phonon transmissivity obtained from different GBs leads to a very small variation of the estimated thermal conductivity of polycrystalline $MoS_2$, although the TBC of S4|4 and Mo4|8 differs noticeably. Based on our simulation results, we suggest that polycrystalline samples of $MoS_2$ with the same grain size may have similar thermal conductivities even with different GBs. Furthermore, it should be emphasized that the Casimir model begins to match the GB model when the grain size is greater than 500 nm. In such a diffusive transport regime, the intrinsic phonon−phonon scattering is the dominating mechanism. In contrast, when the grain size is smaller than 50 nm, pronounced ballistic phonon transport through GBs plays an important role and must be captured by including the detailed information of phonon transmission through GBs as done in the GB model.

In a recent experimental study,[45] ultralow thermal conductivities of CVD grown polycrystalline $MoS_2$ thin films with grain size of 2−6 nm have been reported. The measured thermal conductivity of polycrystalline $MoS_2$ thin film with the thickness of 3 nm and grain size of 6 nm was only 2 W $m^{-1}$ $K^{-1}$, more than 3 times lower than our calculated value of 6.9 W $m^{-1}$ $K^{-1}$. This discrepancy may result from additional phonon-defect scattering by isotopic and other impurities in their samples. Besides, the much lower thermal conductivity of multilayer $MoS_2$ single crystal, i.e., 44−50 and 48−52 W $m^{-1}$ $K^{-1}$ for four- and seven-layer $MoS_2$ samples[49] due to the weak van der Waals interaction between different layers, could be another reason for such a discrepancy. Previous theoretical simulations on the thermal conductivity of polycrystalline $MoS_2$ mainly resorted to finite-element modeling by either fitting the experiment results[45] or taking the TBC from MD simulations.[50] Their models lack the detailed structural information of the diverse topological dislocations and GBs in polycrystalline $MoS_2$ and the pivotal frequency-dependent phonon properties and thus give rise to much larger discrepancies compared to the experimental results. In contrast, our results from realistic polycrystalline model using the Voronoi method and the GB model by including the frequency-dependent phonon transmissivity can provide a deep microscopic understanding of the thermal transport in polycrystalline $MoS_2$, shedding new lights on tailoring the thermal conductivity of polycrystalline materials via the mode-by-mode phonon−GB interaction.

## CONCLUSIONS

In summary, we systematically performed NEMD simulations and atomic Green's function calculations to investigate the phonon−GB interaction and thermal transport in polycrystalline $MoS_2$. The chosen twelve structures of stable GBs in polycrystalline $MoS_2$ provide a reasonable range of TBC (ranging from $6.4 \times 10^8$ W $m^{-2}$ $K^{-1}$ of Mo4|8 to $35.3 \times 10^8$ W $m^{-2}$ $K^{-1}$ of Mo-sh.ch. and S4|4), which is significantly lower than those of graphene and h-BN. By analyzing the vibrations and energy of GBs, it is found that the TBC of GBs presents a negative correlation with the GB energy and is positively related to the VDOS overlap. Furthermore, from phonon transmission analysis, the GBs can strongly scatter the phonons with frequency larger than roughly 2 THz, below which the phonons are nearly free of GB scattering. The structure disorder induced by dense GBs also results in the pronounced phonon localization effect in the middle- and high-frequency region, strikingly reducing the phonon group velocities and impeding the effective thermal transport in polycrystalline $MoS_2$. Finally, we predicted the thermal conductivity of polycrystalline $MoS_2$ as a function of grain size. The thermal conductivity of realistic polycrystalline $MoS_2$ is well below the results from the Casimir model. By taking into account the phonon transmission information at GBs, our results from the analytical GB model gave a very good agreement with those from direct NEMD simulations, which could help to understand the phonon−GB interaction in other polycrystalline materials in the future. Our simulations provide a deep understanding of the underlying mechanisms of the phonon−GB interaction in polycrystalline $MoS_2$ and demonstrate the possibility to engineer material properties with controlled polycrystalline structures for efficient thermoelectric and thermal management applications.

## ASSOCIATED CONTENT

### Supporting Information

The Supporting Information is available free of charge on the ACS Publications website at DOI: 10.1021/acsami.9b06196.

Grain boundary geometries in polycrystalline $MoS_2$ (Section I); thermal-transport properties of the pristine $MoS_2$ monolayer (Section II); phonon spectral energy density analysis (Section III); atomic Green's function method (Section IV); phonon transmission analysis for other grain boundaries (Section V); participation ratio and phonon group velocity for other grain boundaries (Section VI); and construction of polycrystalline $MoS_2$ by Voronoi algorithm (Section VII) (PDF)

## AUTHOR INFORMATION


### Corresponding Authors

*E-mail: chenxiaobin@hit.edu.cn (X.C.).
*E-mail: xlzou@sz.tsinghua.edu.cn (X.Z.).

### ORCID

Xiaobin Chen: 0000-0001-5761-5020
Xiaolong Zou: 0000-0002-3987-6865


### Notes

The authors declare no competing financial interest.



DOI: 10.1021/acsami.9b06196
ACS Appl. Mater. Interfaces 2019, 11, 25547−25555

## ■ ACKNOWLEDGMENTS

This work was supported by NSF-China (Grant No. 11704257 (X.C.)), Shenzhen Basic Research Projects (No. JCYJ20170407155608882), the Economic, Trade and Information Commission of Shenzhen Municipality for the 2017 Graphene Manufacturing Innovation Center Project (No. 201901171523), Guangdong Innovative and Entrepreneurial Research Team Program (Grant No. 2017ZT07C341), the Development and Reform Commission of Shenzhen Municipality under the "Low Dimensional Materials and Devices Discipline", the Youth 1000-Talent Program of China, and the Tsinghua-Berkeley Shenzhen Institute (TBSI). C.L. would like to thank Prof. Xiaoliang Zhang (Dalian University of Technology), Dr Yanguang Zhou (University of California, Los Angeles), and Dr Lei Feng (The University of Tokyo) for helpful discussions.

## ■ REFERENCES

(1) Moore, A. L.; Shi, L. Emerging challenges and materials for thermal management of electronics. *Mater. Today* **2014**, *17*, 163−174.
(2) Hopkins, P. E. Thermal transport across solid interfaces with nanoscale imperfections: effects of roughness, disorder, dislocations, and bonding on thermal boundary conductance. *ISRN Mech. Eng.* **2013**, *2013*, 1−19.
(3) Callaway, J.; von Baeyer, H. C. Effect of Point Imperfections on Lattice Thermal Conductivity. *Phys. Rev.* **1960**, *120*, 1149−1154.
(4) Chen, Z.; Zhang, X.; Pei, Y. Manipulation of Phonon Transport in Thermoelectrics. *Adv. Mater.* **2018**, *30*, No. 1705617.
(5) Chen, Z.; Jian, Z.; Li, W.; Chang, Y.; Ge, B.; Hanus, R.; Yang, J.; Chen, Y.; Huang, M.; Snyder, G. J.; Pei, Y. Lattice Dislocations Enhancing Thermoelectric PbTe in Addition to Band Convergence. *Adv. Mater.* **2017**, *29*, No. 1606768.
(6) Zhang, H.; Lee, G.; Cho, K. Thermal transport in graphene and effects of vacancy defects. *Phys. Rev. B* **2011**, *84*, No. 115460.
(7) Peng, B.; Ning, Z.; Zhang, H.; Shao, H.; Xu, Y.; Ni, G.; Zhu, H. Beyond Perturbation: Role of Vacancy-Induced Localized Phonon States in Thermal Transport of Monolayer MoS2. *J. Phys. Chem. C* **2016**, *120*, 29324−29331.
(8) Bagri, A.; Kim, S. P.; Ruoff, R. S.; Shenoy, V. B. Thermal transport across twin grain boundaries in polycrystalline graphene from nonequilibrium molecular dynamics simulations. *Nano Lett.* **2011**, *11*, 3917−3921.
(9) Sadasivam, S.; Ye, N.; Feser, J. P.; Charles, J.; Miao, K.; Kubis, T.; Fisher, T. S. Thermal transport across metal silicide-silicon interfaces: First-principles calculations and Green's function transport simulations. *Phys. Rev. B* **2017**, *95*, No. 085310.
(10) Mingo, N.; Stewart, D. A.; Broido, D. A.; Srivastava, D. Phonon transmission through defects in carbon nanotubes from first principles. *Phys. Rev. B* **2008**, *77*, No. 033418.
(11) Katcho, N. A.; Carrete, J.; Li, W.; Mingo, N. Effect of nitrogen and vacancy defects on the thermal conductivity of diamond: An ab initio Green's function approach. *Phys. Rev. B* **2014**, *90*, No. 094117.
(12) Ding, Z.; Pei, Q.-X.; Jiang, J.-W.; Zhang, Y.-W. Manipulating the Thermal Conductivity of Monolayer MoS2 via Lattice Defect and Strain Engineering. *J. Phys. Chem. C* **2015**, *119*, 16358−16365.
(13) Liu, X.; Zhang, G.; Zhang, Y. W. Topological Defects at the Graphene/h-BN interface Abnormally Enhance Its Thermal Conductance. *Nano Lett.* **2016**, *16*, 4954−4959.
(14) Chen, X.; Xiong, L.; Chernatynskiy, A.; Chen, Y. A molecular dynamics study of tilt grain boundary resistance to slip and heat transfer in nanocrystalline silicon. *J. Appl. Phys.* **2014**, *116*, No. 244309.
(15) Chen, X.; Li, W.; Xiong, L.; Li, Y.; Yang, S.; Zheng, Z.; McDowell, D. L.; Chen, Y. Ballistic-diffusive phonon heat transport across grain boundaries. *Acta Mater.* **2017**, *136*, 355−365.
(16) Lim, J.; Hippalgaonkar, K.; Andrews, S. C.; Majumdar, A.; Yang, P. Quantifying surface roughness effects on phonon transport in silicon nanowires. *Nano Lett.* **2012**, *12*, 2475−2482.
(17) Kim, K. S.; Kim, Y. M.; Mun, H.; Kim, J.; Park, J.; Borisevich, A. Y.; Lee, K. H.; Kim, S. W. Direct Observation of Inherent Atomic-Scale Defect Disorders responsible for High-Performance Ti1-x Hfx NiSn1-y Sby Half-Heusler Thermoelectric Alloys. *Adv. Mater.* **2017**, *29*, No. 1702091.
(18) Giri, A.; King, S. W.; Lanford, W. A.; Mei, A. B.; Merrill, D.; Li, L.; Oviedo, R.; Richards, J.; Olson, D. H.; Braun, J. L.; Gaskins, J. T.; Deangelis, F.; Henry, A.; Hopkins, P. E. Interfacial Defect Vibrations Enhance Thermal Transport in Amorphous Multilayers with Ultrahigh Thermal Boundary Conductance. *Adv. Mater.* **2018**, *30*, No. 1804097.
(19) Zhou, C.; Lee, Y. K.; Cha, J.; Yoo, B.; Cho, S. P.; Hyeon, T.; Chung, I. Defect Engineering for High-Performance n-Type PbSe Thermoelectrics. *J. Am. Chem. Soc.* **2018**, *140*, 9282−9290.
(20) Lee, S. M.; Cahill, D. G.; Venkatasubramanian, R. Thermal conductivity of Si−Ge superlattices. *Appl. Phys. Lett.* **1997**, *70*, 2957−2959.
(21) Joshi, G.; Lee, H.; Lan, Y.; Wang, X.; Zhu, G.; Wang, D.; Gould, R. W.; Cuff, D. C.; Tang, M. Y.; Dresselhaus, M. S.; et al. Enhanced thermoelectric figure-of-merit in nanostructured p-type silicon germanium bulk alloys. *Nano Lett.* **2008**, *8*, 4670−4674.
(22) Poudel, B.; Hao, Q.; Ma, Y.; Lan, Y.; Minnich, A.; Yu, B.; Yan, X.; Wang, D.; Muto, A.; Vashaee, D.; et al. High-thermoelectric performance of nanostructured bismuth antimony telluride bulk alloys. *Science* **2008**, *320*, 634−638.
(23) Deng, R.; Su, X.; Zheng, Z.; Liu, W.; Yan, Y.; Zhang, Q.; Dravid, V. P.; Uher, C.; Kanatzidis, M. G.; Tang, X. Thermal conductivity in Bi0.5Sb1.5Te3+x and the role of dense dislocation arrays at grain boundaries. *Sci. Adv.* **2018**, *4*, No. eaar5606.
(24) Kim, S. I.; Lee, K. H.; Mun, H. A.; Kim, H. S.; Hwang, S. W.; Roh, J. W.; Yang, D. J.; Shin, W. H.; Li, X. S.; Lee, Y. H. Dense dislocation arrays embedded in grain boundaries for high-performance bulk thermoelectrics. *Science* **2015**, *348*, 109−114.
(25) Klemens, P. G. The Scattering of Low-Frequency Lattice Waves by Static Imperfections. *Proc. Phys. Soc., London, Sect. A* **1955**, *68*, 1113−1128.
(26) Carruthers, P. Scattering of phonons by elastic strain fields and the thermal resistance of dislocations. *Phys. Rev.* **1959**, *114*, 995−1001.
(27) Ninomiya, T. Dislocation vibration and phonon scattering. *J. Phys. Soc. Jpn.* **1968**, *25*, 830−840.
(28) Li, M.; Ding, Z.; Meng, Q.; Zhou, J.; Zhu, Y.; Liu, H.; Dresselhaus, M. S.; Chen, G. Nonperturbative Quantum Nature of the Dislocation-Phonon Interaction. *Nano Lett.* **2017**, *17*, 1587−1594.
(29) Chen, X.; Xiong, L.; McDowell, D. L.; Chen, Y. Effects of phonons on mobility of dislocations and dislocation arrays. *Scripta Mater.* **2017**, *137*, 22−26.
(30) Xiong, L.; McDowell, D. L.; Chen, Y. Sub-THz Phonon drag on dislocations by coarse-grained atomistic simulations. *Int. J. Plast.* **2014**, *55*, 268−278.
(31) Feser, J. P.; Chan, E. M.; Majumdar, A.; Segalman, R. A.; Urban, J. J. Ultralow thermal conductivity in polycrystalline CdSe thin films with controlled grain size. *Nano Lett.* **2013**, *13*, 2122−2127.
(32) Chen, C.-L.; Wang, H.; Chen, Y.-Y.; Day, T.; Snyder, G. J. Thermoelectric properties of p-type polycrystalline SnSe doped with Ag. *J. Mater. Chem. A* **2014**, *2*, 11171−11176.
(33) Oyake, T.; Feng, L.; Shiga, T.; Isogawa, M.; Nakamura, Y.; Shiomi, J. Ultimate Confinement of Phonon Propagation in Silicon Nanocrystalline Structure. *Phys. Rev. Lett.* **2018**, *120*, No. 045901.
(34) Zhou, Y.; Hu, M. Record Low Thermal Conductivity of Polycrystalline Si Nanowire: Breaking the Casimir Limit by Severe Suppression of Propagons. *Nano Lett.* **2016**, *16*, 6178−6187.
(35) Cai, Z.; Liu, B.; Zou, X.; Cheng, H. M. Chemical Vapor Deposition Growth and Applications of Two-Dimensional Materials and Their Heterostructures. *Chem. Rev.* **2018**, *118*, 6091−6133.


DOI: 10.1021/acsami.9b06196
*ACS Appl. Mater. Interfaces* 2019, 11, 25547−25555

(36) Zou, X.; Liu, Y.; Yakobson, B. I. Predicting dislocations and grain boundaries in two-dimensional metal-disulfides from the first principles. *Nano Lett.* **2013**, *13*, 253−258.
(37) Zou, X.; Yakobson, B. I. Metallic High-Angle Grain Boundaries in Monolayer Polycrystalline WS2. *Small* **2015**, *11*, 4503−4507.
(38) Zhou, W.; Zou, X.; Najmaei, S.; Liu, Z.; Shi, Y.; Kong, J.; Lou, J.; Ajayan, P. M.; Yakobson, B. I.; Idrobo, J.-C. Intrinsic Structural Defects in Monolayer Molybdenum Disulfide. *Nano Lett.* **2013**, *13*, 2615−2622.
(39) Azizi, A.; Zou, X.; Ercius, P.; Zhang, Z.; Elias, A. L.; Perea-Lopez, N.; Stone, G.; Terrones, M.; Yakobson, B. I.; Alem, N. Dislocation motion and grain boundary migration in two-dimensional tungsten disulphide. *Nat. Commun.* **2014**, *5*, No. 4867.
(40) Najmaei, S.; Liu, Z.; Zhou, W.; Zou, X.; Shi, G.; Lei, S.; Yakobson, B. I.; Idrobo, J. C.; Ajayan, P. M.; Lou, J. Vapour phase growth and grain boundary structure of molybdenum disulphide atomic layers. *Nat. Mater.* **2013**, *12*, 754−759.
(41) Zou, X.; Liu, M.; Shi, Z.; Yakobson, B. I. Environment-Controlled Dislocation Migration and Superplasticity in Monolayer MoS2. *Nano Lett.* **2015**, *15*, 3495−3500.
(42) Wu, J.; Cao, P.; Zhang, Z.; Ning, F.; Zheng, S.; He, J.; Zhang, Z. Grain-size Controlled Mechanical Properties of Polycrystalline Monolayer MoS2. *Nano Lett.* **2018**, *18*, 1543−1552.
(43) Wu, J.; Gong, H.; Zhang, Z.; He, J.; Ariza, P.; Ortiz, M.; Zhang, Z. Topology and polarity of dislocation cores dictate the mechanical strength of monolayer MoS2. *Appl. Mater. Today* **2019**, *15*, 34−42.
(44) Zhang, Z.; Zou, X.; Crespi, V. H.; Yakobson, B. I. Intrinsic Magnetism of Grain Boundaries in Two-Dimensional Metal Dichalcogenides. *ACS Nano* **2013**, *7*, 10475−10481.
(45) Sledzinska, M.; Quey, R.; Mortazavi, B.; Graczykowski, B.; Placidi, M.; Saleta Reig, D.; Navarro-Urrios, D.; Alzina, F.; Colombo, L.; Roche, S.; Sotomayor Torres, C. M. Record Low Thermal Conductivity of Polycrystalline MoS2 Films: Tuning the Thermal Conductivity by Grain Orientation. *ACS Appl. Mater. Interfaces* **2017**, *9*, 37905−37911.
(46) Sledzinska, M.; Graczykowski, B.; Placidi, M.; Reig, D. S.; Sachat, A. E.; Reparaz, J. S.; Alzina, F.; Mortazavi, B.; Quey, R.; Colombo, L.; Roche, S.; Torres, C. M. S. Thermal conductivity of MoS2 polycrystalline nanomembranes. *2D Mater.* **2016**, *3*, No. 035016.
(47) Zhang, X.; Sun, D.; Li, Y.; Lee, G. H.; Cui, X.; Chenet, D.; You, Y.; Heinz, T. F.; Hone, J. C. Measurement of Lateral and Interfacial Thermal Conductivity of Single- and Bilayer MoS2 and MoSe2 Using Refined Optothermal Raman Technique. *ACS Appl. Mater. Interfaces* **2015**, *7*, 25923−25929.
(48) Sahoo, S.; Gaur, A. P. S.; Ahmadi, M.; Guinel, M. J. F.; Katiyar, R. S. Temperature-Dependent Raman Studies and Thermal Conductivity of Few-Layer MoS2. *J. Phys. Chem. C* **2013**, *117*, 9042−9047.
(49) Jo, I.; Pettes, M. T.; Ou, E.; Wu, W.; Shi, L. Basal-plane thermal conductivity of few-layer molybdenum disulfide. *Appl. Phys. Lett.* **2014**, *104*, No. 201902.
(50) Mortazavi, B.; Quey, R.; Ostadhossein, A.; Villani, A.; Moulin, N.; van Duin, A. C. T.; Rabczuk, T. Strong thermal transport along polycrystalline transition metal dichalcogenides revealed by multiscale modeling for MoS2. *Appl. Mater. Today* **2017**, *7*, 67−76.
(51) Ostadhossein, A.; Rahnamoun, A.; Wang, Y.; Zhao, P.; Zhang, S.; Crespi, V. H.; van Duin, A. C. T. ReaxFF Reactive Force-Field Study of Molybdenum Disulfide (MoS2). *J. Phys. Chem. Lett.* **2017**, *8*, 631−640.
(52) Casimir, H. B. G. Note on the conduction of heat in crystals. *Physica* **1938**, *5*, 495−500.
(53) Shindé, S. L.; Srivastava, G. P. *Length-Scale Dependent Phonon Interactions*; Springer: NY, 2014.
(54) Hirel, P. Atomsk: a tool for manipulating and converting atomic data files. *Comput. Phys. Commun.* **2015**, *197*, 212−219.
(55) Wang, S.; Lee, G.-D.; Lee, S.; Yoon, E.; Warner, J. H. Detailed atomic reconstruction of extended line defects in monolayer MoS2. *ACS Nano* **2016**, *10*, 5419−5430.
(56) Lin, J.; Pantelides, S. T.; Zhou, W. Vacancy-induced formation and growth of inversion domains in transition-metal dichalcogenide monolayer. *ACS Nano* **2015**, *9*, 5189−5197.
(57) Plimpton, S. Fast parallel algorithms for short-range molecular dynamics. *J. Comput. Phys.* **1995**, *117*, 1−19.
(58) Liang, T.; Phillpot, S. R.; Sinnott, S. B. Parametrization of a reactive many-body potential for Mo−S systems. *Phys. Rev. B* **2009**, *79*, No. 245110.
(59) Liang, T.; Phillpot, S. R.; Sinnott, S. B. Erratum: Parametrization of a reactive many-body potential for Mo−S systems [Phys. Rev. B79, 245110 (2009)]. *Phys. Rev. B* **2012**, *85*, No. 199903.
(60) Nosé, S. A unified formulation of the constant temperature molecular dynamics methods. *J. Chem. Phys.* **1984**, *81*, 511−519.
(61) Hoover, W. G. Canonical dynamics: Equilibrium phase-space distributions. *Phys. Rev. A* **1985**, *31*, 1695−1697.
(62) Hong, Y.; Zhang, J.; Zeng, X. C. Thermal Conductivity of Monolayer MoSe2 and MoS2. *J. Phys. Chem. C* **2016**, *120*, 26067−26075.
(63) Thomas, J. A.; Turney, J. E.; Iutzi, R. M.; Amon, C. H.; McGaughey, A. J. H. Predicting phonon dispersion relations and lifetimes from the spectral energy density. *Phys. Rev. B* **2010**, *81*, No. 081411.
(64) Larkin, J. M.; Turney, J. E.; Massicotte, A. D.; Amon, C. H.; McGaughey, A. J. H. Comparison and Evaluation of Spectral Energy Methods for Predicting Phonon Properties. *J. Comput. Theor. Nanosci.* **2014**, *11*, 249−256.
(65) Li, W.; Carrete, J.; Mingo, N. Thermal conductivity and phonon linewidths of monolayer MoS2 from first principles. *Appl. Phys. Lett.* **2013**, *103*, No. 253103.
(66) Cai, Y.; Lan, J.; Zhang, G.; Zhang, Y.-W. Lattice vibrational modes and phonon thermal conductivity of monolayer MoS2. *Phys. Rev. B* **2014**, *89*, No. 035438.
(67) Zou, J.; Kotchetkov, D.; Balandin, A. A.; Florescu, D. I.; Pollak, F. H. Thermal conductivity of GaN films: Effects of impurities and dislocations. *J. Appl. Phys.* **2002**, *92*, 2534−2539.
(68) Ni, Y.; Xiong, S.; Volz, S.; Dumitric, T. Thermal transport along the dislocation line in silicon carbide. *Phys. Rev. Lett.* **2014**, *113*, No. 124301.
(69) Sellan, D. P.; Landry, E. S.; Turney, J. E.; McGaughey, A. J. H.; Amon, C. H. Size effects in molecular dynamics thermal conductivity predictions. *Phys. Rev. B* **2010**, *81*, No. 214305.
(70) McGaughey, A. J.; Kaviany, M. Phonon transport in molecular dynamics simulations: formulation and thermal conductivity prediction. *Adv. Heat Transfer* **2006**, *39*, 169−255.
(71) Li, B.; Lan, J.; Wang, L. Interface thermal resistance between dissimilar anharmonic lattices. *Phys. Rev. Lett.* **2005**, *95*, No. 104302.
(72) Lin, C.; Zhang, X.; Rao, Z. Theoretical prediction of thermal transport in BC2N monolayer. *Nano Energy* **2017**, *38*, 249−256.
(73) English, T. S.; Duda, J. C.; Smoyer, J. L.; Jordan, D. A.; Norris, P. M.; Zhigilei, L. V. Enhancing and tuning phonon transport at vibrationally mismatched solid-solid interfaces. *Phys. Rev. B* **2012**, *85*, No. 035438.
(74) Losego, M. D.; Grady, M. E.; Sottos, N. R.; Cahill, D. G.; Braun, P. V. Effects of chemical bonding on heat transport across interfaces. *Nat. Mater.* **2012**, *11*, 502−506.
(75) Hodson, S. L.; Bhuvana, T.; Cola, B. A.; Xu, X.; Kulkarni, G.; Fisher, T. S. Palladium thiolate bonding of carbon nanotube thermal interfaces. *J. Electron. Packag.* **2011**, *133*, No. 020907.
(76) Mortazavi, B.; Pereira, L. F.; Jiang, J. W.; Rabczuk, T. Modelling heat conduction in polycrystalline hexagonal boron-nitride films. *Sci. Rep.* **2015**, *5*, No. 13228.
(77) Xu, Y.; Chen, X.; Gu, B.-L.; Duan, W. Intrinsic anisotropy of thermal conductance in graphene nanoribbons. *Appl. Phys. Lett.* **2009**, *95*, No. 233116.
(78) Chen, X.; Liu, Y.; Duan, W. Thermal Engineering in Low-Dimensional Quantum Devices: A Tutorial Review of Nonequilibrium Green's Function Methods. *Small Methods* **2018**, *2*, No. 1700343.


DOI: 10.1021/acsami.9b06196
*ACS Appl. Mater. Interfaces* 2019, 11, 25547−25555

(79) Xu, Y.; Chen, X.; Wang, J.-S.; Gu, B.-L.; Duan, W. Thermal transport in graphene junctions and quantum dots. *Phys. Rev. B* **2010**, *81*, No. 195425.
(80) Seyf, H. R.; Henry, A. A method for distinguishing between propagons, diffusions, and locons. *J. Appl. Phys.* **2016**, *120*, No. 025101.
(81) Allen, P. B.; Feldman, J. L.; Fabian, J.; Wooten, F. Diffusons, locons and propagons: Character of atomic vibrations in amorphous Si. *Philos. Mag. B* **1999**, *79*, 1715−1731.
(82) Wang, Z.; Alaniz, J. E.; Jang, W.; Garay, J. E.; Dames, C. Thermal conductivity of nanocrystalline silicon: importance of grain size and frequency-dependent mean free paths. *Nano Lett.* **2011**, *11*, 2206−2213.
(83) Dames, C.; Chen, G. Theoretical phonon thermal conductivity of Si/Ge superlattice nanowires. *J. Appl. Phys.* **2004**, *95*, 682−693.
(84) Qin, G.; Zhang, X.; Yue, S.-Y.; Qin, Z.; Wang, H.; Han, Y.; Hu, M. Resonant bonding driven giant phonon anharmonicity and low thermal conductivity of phosphorene. *Phys. Rev. B* **2016**, *94*, No. 165445.
(85) Ziman, J. M. *Electrons and Phonons: The Theory of Transport Phenomena in Solids*; Oxford University Press: London, 1960.



DOI: 10.1021/acsami.9b06196
*ACS Appl. Mater. Interfaces* 2019, 11, 25547−25555